

The formation and evolution of a diffusive interface

By M. JEROEN MOLEMAKER AND HENK A. DIJKSTRA

Institute for Marine and Atmospheric Research, Department of Physics and Astronomy,
University of Utrecht, Prinsentopplein 5, 3584 CC, Utrecht, The Netherlands

(Received 26 January 1995 and in revised form 16 August 1996)

The formation and evolution of a diffusive interface in a stable salt-stratified layer cooled from above is studied in a two-dimensional geometry by direct numerical simulation. For a typical example with realistic parameters, the evolution of the flow is computed up to the moment where three layers can be distinguished. Focus is on the development of the first mixed layer. The convective velocity scaling as proposed by Hunt (1984) and previously proposed expressions for the interfacial heat flux (Huppert 1971; Fernando 1989*a*) are shown to correspond well with the results of the simulation. The evolution of the first layer can be well described by an entrainment relation based on a local balance between kinetic and potential energy with mixing efficiency γ . The new entrainment relation is shown to fit the numerical results well and an interpretation of γ in terms of the overall energy balances of the flow is given.

Previously, two rival mechanisms have been proposed that determine the final thickness of the first layer (Turner 1968; Fernando 1987). One of the distinguishing features of both mechanisms is whether a transition in entrainment regime – as the first layer develops – is a necessary condition for the mixed layer to stop growing. Another is the presence of a buoyancy jump over the interface before substantial convection in the second layer occurs. From the numerical results, we find a significant buoyancy jump even before the thermal boundary layer ahead of the first layer becomes unstable. Moreover, the convective activity in the second layer is too small to be able to stop the growth of the first layer. We therefore favour the view proposed by Fernando (1987) that a transition in entrainment regime determines the thickness of the first layer. Following this, a new one-dimensional model of layer formation is proposed. Important expressions within this model are verified using the results of the numerical simulation. The model contains two constants which are determined from the numerical results. The results of the new model fit experimental results quite well and the parameter dependence of the thickness of the first layer is not sensitive to the values of the two constants.

1. Introduction

Layer formation is a characteristic feature of double-diffusive convection which may occur in stably stratified liquids in which two substances, e.g. heat and salt, diffuse at a different rate. The presence of these convecting layers may enhance the transport of each component significantly. Double-diffusive convection is therefore a potentially important transport mechanism, e.g. for heat and salt in the ocean (Schmitt 1994) and for different components in a magma chamber (Huppert & Turner 1981). However, it has always been a sort of curiosity in oceanography. There

is overwhelming evidence of signatures of these processes in the ocean, for example the step structures in temperature and salinity in thermohaline staircases (Fernando 1989b). On the other hand, there is no clear indication that these effects form a really important contribution to the mixing of heat and salt in the ocean on a larger scale. As far as we know, there are no studies explicitly incorporating the effect of the processes, e.g. in terms of a subgrid model, in larger scale models. In the latter models, the mixing coefficients for heat and salt are therefore usually taken equal. However, recent studies (Gargett & Holloway 1992) have shown that the large-scale circulation is sensitive to the ratio of mixing coefficients.

Layer formation typically occurs when a vertical temperature gradient is imposed on an initially vertical salinity gradient. When the fastest diffusing substance is (de)stabilizing, layers may form through (diffusive) finger instabilities (Huppert & Linden 1979; Turner & Stommel 1964). In this paper, we consider layer formation in the 'diffusive' favourable case. A typical experiment consists of heating a liquid, which has constant temperature but otherwise is stably stratified through a constant salt gradient dS_0/dz , from below (Turner 1968). A constant heat flux \mathcal{H} [Wm^{-2}] is applied to the bottom of the liquid. First a well-mixed layer develops near the bottom and the thickness of this layer grows with time. After a while, a second layer develops which is separated from the first by a relatively sharp interface. Subsequently, this process repeats and a series of well-mixed layers develops separated by sharp (diffusive) interfaces.

Let ρ_0 [kg m^{-3}], C_p [$\text{J kg}^{-1} \text{K}^{-1}$] and α [K^{-1}] indicate the reference density, the specific heat and the coefficient of thermal expansion of the liquid, respectively. The buoyancy flux q_0 [m^2s^{-3}] which is applied to the bottom of the liquid is then given by

$$q_0 = \frac{g\alpha\mathcal{H}}{\rho_0 C_p} \quad (1.1)$$

where g is the gravitational acceleration. The other quantities important in describing the physics of the layer formation are the coefficient of salinity contraction β , the initial constant salinity gradient dS_0/dz and the thermal and solutal diffusion coefficients κ and D . In experiments (Fernando 1987; Huppert & Linden 1979; Turner 1968), it is found that the thickness of the first mixed layer, say h^* , increases approximately proportional to the square root of time. After some time, the growth rate decreases and at a time t_c^* , the thickness of the first layer is nearly constant in time. Experiments indicate that this final layer thickness, from now on indicated by h_f^* , is proportional to a power n of q_0 and a power m of the buoyancy frequency N , where $N^2 = -g\beta dS_0/dz$. Turner (1968) could fit the experimental data with $n = 3/4$, $m = -2$ while Fernando (1987) was able to do this with $n = 1/2$, $m = -3/2$. With respect to ocean mixing, the scaling of the layer thickness is central to the determination of the mixing coefficients (Kelley 1984; Fernando 1989b). Heat and salt fluxes across the interfaces in a thermohaline staircase can be expressed in terms of the temperature and salinity differences over the interface. These differences can be expressed in terms of the layer thickness if the background profiles of temperature and salinity are assumed to be locally linear.

Both Fernando (1987) and Turner (1968) provide a physical picture of the evolution of the first layer and the formation of the second layer. Turner assumes the buoyancy jump over the interface that separates the first layer from the ambient liquid to be zero, i.e. the interface is always marginally stable. When the heat loss through the interface is neglected, conservation of heat and salt over the liquid layer leads to the

following equation for the evolution of the mixed layer depth h^* :

$$h^* = C q_0^{1/2} N^{-1} t^{*1/2} \quad (1.2)$$

where the constant C is equal to $\sqrt{2}$ (Turner 1968). In contrast with Turner, Fernando (1987) allows for a small buoyancy difference between the first layer and the ambient liquid and models the evolution of the mixed layer using an entrainment relation. The latter model also leads to a relation (1.2) but with a constant C different from $\sqrt{2}$. Hence, both models provide similar initial growth rates although the underlying physics is essentially different. Another difference between both models is the explanation of the final layer thickness h_f^* . In Turner (1968), the final layer thickness h_f^* is assumed to be determined by an instability of a thermal boundary layer, which is present just ahead of the interface. As soon as this instability occurs, the first layer stops growing. The latter ideas have also been used by Huppert & Linden (1979), who studied total staircase growth. In Fernando (1987), the thickness h_f^* is assumed to be determined by a balance between the kinetic energy flux of the eddies and potential energy production associated with buoyancy differences in the first layer.

From a theoretical point of view, the description of the physics of the evolution of the first layer is unsatisfactory. The physics in both models is essentially different and the results lead to a different scaling for h_f^* in terms of q_0 and N . Turner has to assume a critical Rayleigh number, which must be taken quite large to fit the experimental data. In Fernando's model, the entrainment relation is only associated with salinity differences whereas temperature differences are neglected. However, in the relation determining the final thickness of the first layer, a buoyancy jump determined by both salinity and temperature differences has to be assumed to obtain a reasonable balance.

In this paper, we study the formation and evolution of the first layer by direct numerical simulation of the governing equations in a two-dimensional geometry. In reality, the flow is obviously three-dimensional but it is believed that a two-dimensional model captures the essential physics of layer formation, which is confirmed by the results. Apart from this, due to the high resolution required, a three-dimensional simulation of these flows would be extremely computationally expensive. A similar (two-dimensional) simulation has been performed by Kazmierczak & Poulikakos (1990) but, due to an insufficient resolution, a multi-layered structure was not found. Using a high-resolution CFD code, a typical example of a stably stratified liquid cooled from above is considered for realistic values of parameters. Preliminary results of these computations were presented in Molemaker & Dijkstra (1995). The results are here analysed extensively for dominant balances and relevant scales. Previously suggested expressions for heat fluxes across diffusive interfaces are compared with the numerical results and shown to give good agreement. An entrainment relation, extending those proposed in Linden, 1975, Turner (1979) and Fernando (1987), is shown to describe the numerical results well.

The processes of the growth of the first layer, the formation of the interface and the appearance of the second layer are intimately linked. The numerical results clearly show that a significant buoyancy jump over the interface ahead of the first layer appears even before the thermal boundary layer ahead of the interface becomes unstable. Moreover, since the convective activity in the second layer is too small to be solely responsible for the decrease in growth rate of the first layer, we favour the view proposed by Fernando (1987) that a transition in entrainment regime eventually determines the thickness of the first layer. The criterion for this transition as given

in Fernando (1987) is best interpreted as a transition Richardson number, rather than an energy balance. A picture of the energy transfer during the evolution of the diffusive interface is provided by monitoring the horizontally averaged and global kinetic and potential energy balances. The transition criterion can also be interpreted as an energy balance using slightly different scales as those in Fernando (1987).

The analysis leads to an improved one-dimensional model of the layer formation process, which contains two parameters. Both parameters are fitted to numerical results and a good fit is obtained at similar values to those estimated from the experimental results. Apart from a different criterion for the final thickness, the model differs from that in Fernando (1987) with respect to the entrainment relation where the heat flux over the diffusive interface and the effect of the temperature difference on the buoyancy jump is taken into account. In addition, the evolution of the temperature in the quiescent layer below the interface is explicitly computed. The one-dimensional model is used to study the parameter dependence of h_f^* as a function of q_0 and N . A power-law dependence with $n = 0.53$ and $m = -1.56$, respectively is found which fits available experimental results very well. This result is not sensitive to the values of the two parameters in the model. Although both exponents are not very different than those given in Fernando (1987), our one-dimensional model gives a better theoretical justification for their use.

2. Formulation

Consider a two-dimensional incompressible liquid, with constant kinematic viscosity ν in a rectangular box of aspect ratio A (ratio of length L to height H). At the top of the liquid a constant heat flux is prescribed which cools the layer from above (figure 1). This set-up is equivalent to that in experiments (Fernando 1987; Huppert & Linden 1979; Turner 1968), where a liquid is heated from below. The governing equations are non-dimensionalized using scales H , H^2/κ , κ/H , T_∞ , S_∞ for length, time, velocity, temperature and salinity. Here, H is the height of the box and T_∞ , S_∞ are reference values of temperature and salinity, respectively. If the horizontal and vertical velocities are u and w , respectively, the dimensionless equations, with the usual Boussinesq approximation and a linear equation of state, become in a stream function–vorticity ($\psi - \omega$) formulation

$$Pr^{-1} \left(\frac{\partial \omega}{\partial t} + u \frac{\partial \omega}{\partial x} + w \frac{\partial \omega}{\partial z} \right) = \nabla^2 \omega + Ra \left(\frac{\partial T}{\partial x} - \lambda \frac{\partial S}{\partial x} \right), \quad (2.1a)$$

$$\omega = -\nabla^2 \psi, \quad (2.1b)$$

$$\frac{\partial T}{\partial t} + u \frac{\partial T}{\partial x} + w \frac{\partial T}{\partial z} = \nabla^2 T, \quad (2.1c)$$

$$\frac{\partial S}{\partial t} + u \frac{\partial S}{\partial x} + w \frac{\partial S}{\partial z} = \tau \nabla^2 S, \quad (2.1d)$$

where $u = \partial \psi / \partial z$, $w = -\partial \psi / \partial x$ and $\omega = \partial w / \partial x - \partial u / \partial z$. Furthermore, T and S are temperature and salinity, Pr is the Prandtl number, τ the inverse Lewis number, Ra the thermal Rayleigh number and λ the buoyancy ratio based on the reference values of salinity and temperature. These parameters are defined as

$$Ra = \frac{g H^3 \alpha T_\infty}{\nu \kappa}, \quad \lambda = \frac{\beta S_\infty}{\alpha T_\infty}, \quad Pr = \frac{\nu}{\kappa}, \quad \tau = \frac{D}{\kappa}. \quad (2.2)$$

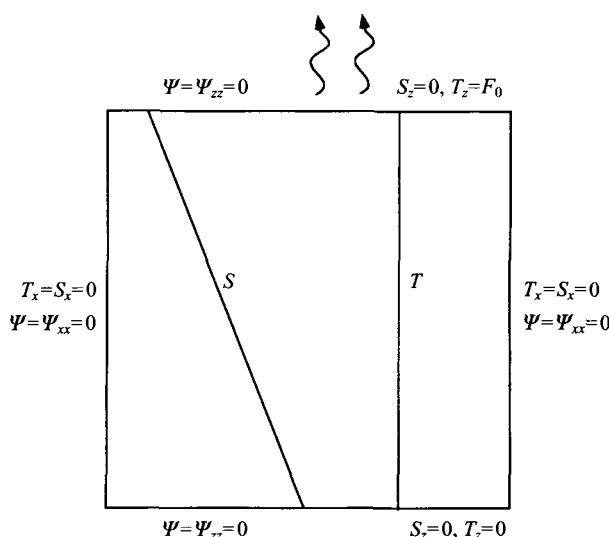


FIGURE 1. Geometrical set-up of the simulation. A two-dimensional container with a stable salt-stratified liquid is cooled from the top.

All boundaries are assumed to be stress-free. At the top wall the salt flux is zero and the heat flux prescribed and equal to \mathcal{H} . All the other walls satisfy no-flux conditions for heat and salt. The dimensionless boundary conditions then become

$$x = 0, A : \quad \psi = \omega = \frac{\partial S}{\partial x} = \frac{\partial T}{\partial x} = 0, \quad (2.3a)$$

$$z = 0 : \quad \psi = \omega = \frac{\partial S}{\partial z} = \frac{\partial T}{\partial z} = 0, \quad (2.3b)$$

$$z = 1 : \quad \psi = \omega = \frac{\partial S}{\partial z} = 0, \quad \frac{\partial T}{\partial z} = F_0, \quad (2.3c)$$

where F_0 is the dimensionless heat flux, given by

$$F_0 = \frac{q_0 H}{g \alpha T_\infty \kappa}. \quad (2.3d)$$

A classical explicit Euler method is used as time discretization and central differences are used as space discretization on an equidistant grid for $i = 0, \dots, N; j = 0, \dots, M$. This scheme is second-order accurate in $(\Delta x, \Delta z)$ and first-order accurate in Δt . To compute the solution at a new time level, first Euler time stepping is performed for ω , T and S and then the Poisson equation (2.1b) is solved for the streamfunction. This explicit formulation enables one to use a very high resolution. A drawback of this method is that, due to numerical stability limitations, the size of the time step is quite severely constrained. The code was verified through comparison with an implicit code (as used in Dijkstra 1988) for several test problems.

3. Results

The parameters Pr and τ are fixed for the water–heat–salt system ($Pr = 7$ and $\tau = 10^{-2}$) and the aspect ratio of the container is set to $A = 1$. In the next subsections the results of a typical run are described and the numerical output analysed.

3.1. A typical example

The simulation follows closely the experiments of Turner (1968), (Huppert & Linden (1979) and Fernando (1987)). The case considered is $Ra = 10^9$, $\lambda = 1$ and a non-dimensional heat flux $F_0 = -4.8$. The numerical resolution used is $N = 200$, $M = 300$. The time step ($\Delta t = 10^{-7}$) and resolution were chosen after extensive testing with different grid sizes and time steps and the resolution used in Kazmierczak & Poulikakos (1990) can be shown to be insufficient. The initial conditions are an isothermal motionless solution with a constant salinity gradient, similar to those realized in laboratory experiments. The choice of the parameters and initial conditions corresponds to the following dimensional values: total depth of the container $H = 10^{-1}$ m, a prescribed buoyancy flux $q_0 = 10^{-6}$ m² s⁻³ and an initial buoyancy frequency $N = 1.12$ s⁻¹. The (constant) values for kinematic viscosity and thermal and saline diffusivity are $\nu = 10^{-6}$ m² s⁻¹, $\kappa = 1.44 \times 10^{-7}$ m² s⁻¹, $D = 1.4 \times 10^{-9}$ m² s⁻¹. The integration in time was continued until a second layer was well established and a third layer started to develop (up to $t^* = 3 \times 10^3$ s). The simulation took about 20 CPU hours on a Cray C98. To make a comparison with experiments easier, the results are presented using dimensional dependent quantities, which all are written with a superscript *. Without this superscript, a dependent quantity is dimensionless.

3.1.1. Growth of the first layer

Due to cooling at the top, the thermal boundary layer becomes unstable and convection rapidly develops, forming a well mixed layer. The evolution of the horizontally averaged salinity, temperature and buoyancy profiles is shown in figure 2(a-c) for several times t^* . Here, the buoyancy B^* is defined as $B^* = g(\rho_0 - \rho^*)/\rho_0 = g(\alpha T^* - \beta S^*)$. In figure 2(d) buoyancy profiles are plotted at many more times, showing more details of the layer formation process.

At $t^* = 70$ s (profiles (i) in figure 2), the first layer starts to develop but both the temperature and salinity profiles in this layer are not yet homogeneous. Both quantities are well-mixed at $t^* = 550$ s (profiles (ii)) and the thickness of the mixed layer increases through turbulent entrainment. The interface, separating the first layer from the liquid below, develops (profiles (iii-v)) but its growth rate decreases with time. From approximately $t^* = 2500$ s (profile (vi)) the thickness of the first layer only changes very slowly. At that time, heat and salt appear well-mixed in the region below the interface and a second mixed layer has developed. In figure 3, the salinity distribution is shown at $t^* = 2750$ s, where light (dark) shading indicates a high (low) salt concentration. The interface separating the two layers can be clearly identified in figure 3 and is located near $z^* = 6.5$ cm.

The parameters of this particular simulation correspond to one of the laboratory experiments in Fernando (1987). The qualitative agreement is good since the same layered structure as in the experiments is found and the thickness of first layer is larger than that of the next layers. More quantitatively, in Fernando (1987) it was found that for $q_0 = 10^{-6}$ m² s⁻³ and $N = 1.12$ s⁻¹, the depth of the first layer is $h_f^* \approx 3.5$ cm (figure 6 in Fernando 1987). This compares well with the result of the numerical simulation where a final depth $h_f^* \approx 3.7$ cm of the first layer is found (figure 2d).

3.1.2. Development of a stable interface

From times larger than $t^* = 500$ s, a certain amount of mixing is present below the interface separating the first layer from the surrounding liquid. At $t^* = 500$ s, the

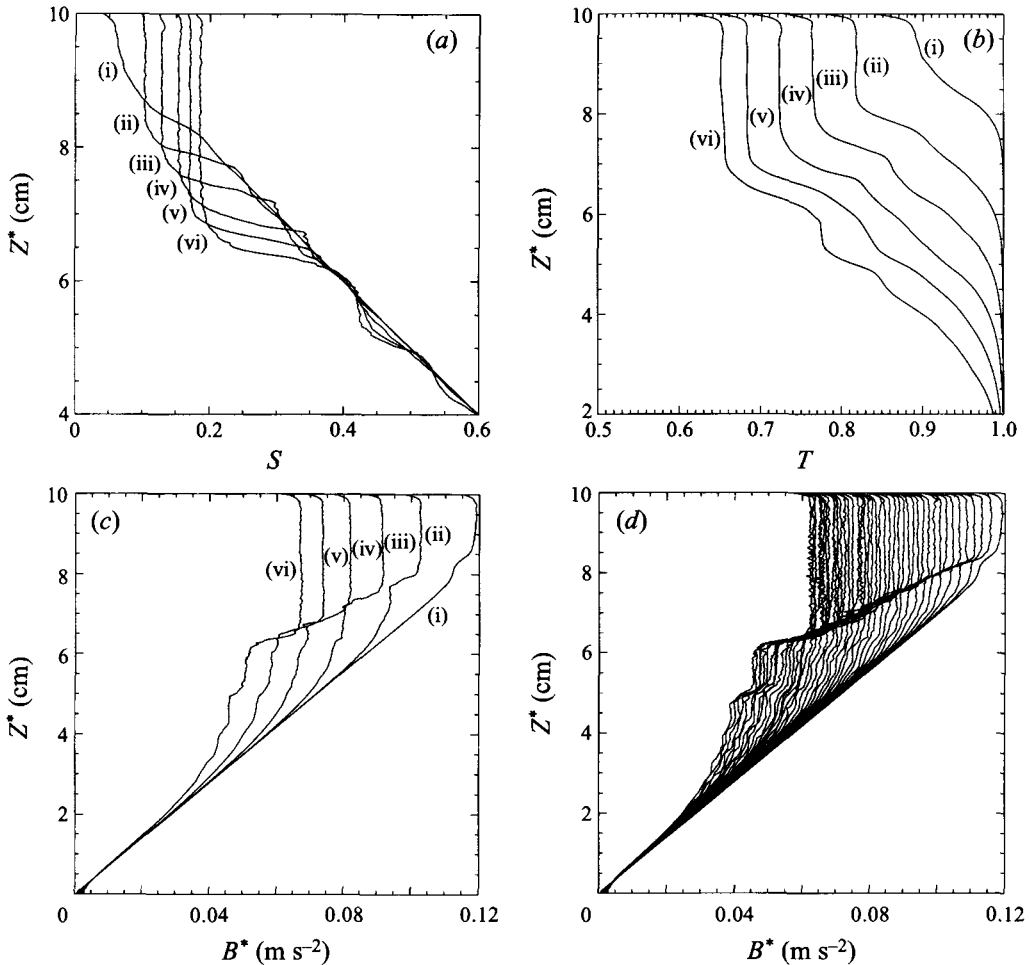


FIGURE 2. Transient development of horizontally averaged profiles. Profiles are shown at (i) $t^* = 70$ s, (ii) $t^* = 550$ s, (iii) $t^* = 1040$ s, (iv) $t^* = 1528$ s, (v) $t^* = 2014$ s and (vi) $t^* = 2500$ s. (a) Salinity S . (b) Temperature T . (c) Buoyancy $B^* = g(\rho_0 - \rho^*)/\rho_0$. (d) Same as (c), but for many more times between $t^* = 70$ and 2920 s. The development and sharpening of the interface is clearly shown as well as the development of a second interface between the second and third layer.

profiles of temperature, salinity and buoyancy are plotted in more detail in figure 4(a). From figure 4(a), an upper bound for the appropriate effective Rayleigh number, based on the thickness of the thermal boundary layer ahead of the interface, is computed as $Ra_e \approx 300$. This value is much smaller than 10^3 , indicating that this boundary layer is still stable. However, again from figure 4(a) one observes that already a significant buoyancy jump has developed. The present calculations consistently show a buoyancy jump that develops over the interface, even when the thermal boundary layer ahead of the interface is stable. This seems to be in contradiction with Huppert & Linden (1979) and Turner (1968) where it is stated that, within experimental accuracy, salt and temperature differences across the interface induce a buoyancy jump that is negligible during the development of the first layer. In Fernando (1987), the small stable buoyancy jump across the interface is estimated to be around 10% of the buoyancy difference due to salt alone. The present results

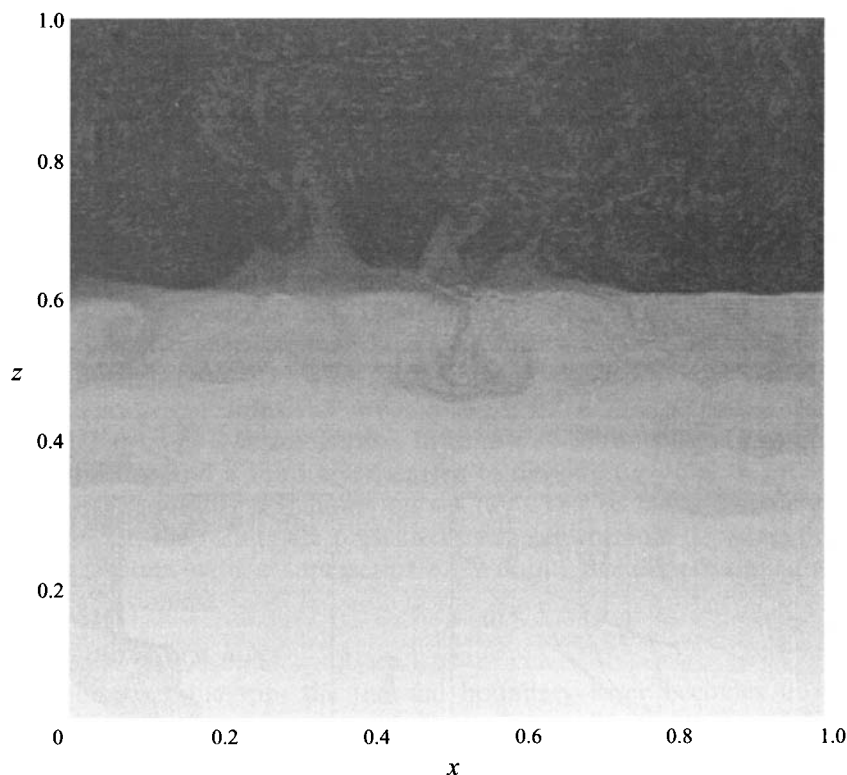


FIGURE 3. Gray-scale plot of the salinity distribution S at $t^* = 2750$ s. Light (dark) shading indicates high (low) salinity.

predict a buoyancy jump that is of the order of 50% of the salinity difference over the interface (figure 2). This buoyancy jump is difficult to determine in experiments since in such a turbulent and intermittent process the position of the interface is not well-defined. Therefore, the question arises whether the buoyancy jump across the stable interface has been underestimated in previous work.

Unfortunately, salinity and temperature profiles from which a buoyancy jump can be calculated are only given in figure 9 in Huppert & Linden (1979), where these are used to show that, within experimental accuracy, no buoyancy jump is present when the first layer grows. This figure has been scanned electronically and the data have been retrieved from the resulting bitmap; it is plotted in figure 4(b). Comparison of figure 4(b) with figure 2(a, b) shows a good (qualitative) correspondence of the profiles. Using the scales indicated in figure 4(b) we can calculate the relative contributions to the density and adding the two profiles we obtain the buoyancy profile shown in figure 4(c). As can be clearly seen, a significant buoyancy jump is present across the interface. The fact that the eye might be deceived in figure 4(b) is due to the different length scales over which salinity and temperature differences occur. From the buoyancy profile in figure 4(c), an estimate is obtained of the buoyancy jump as $\Delta B^* \approx 0.5g\beta S^*$, which is much larger than the estimate of Fernando (1987) but corresponds very well with that found in the present numerical calculations. Hence, although the result as given in figure 9 in Huppert & Linden (1979) is an instantaneous profile and may not show any averaged property over the interface

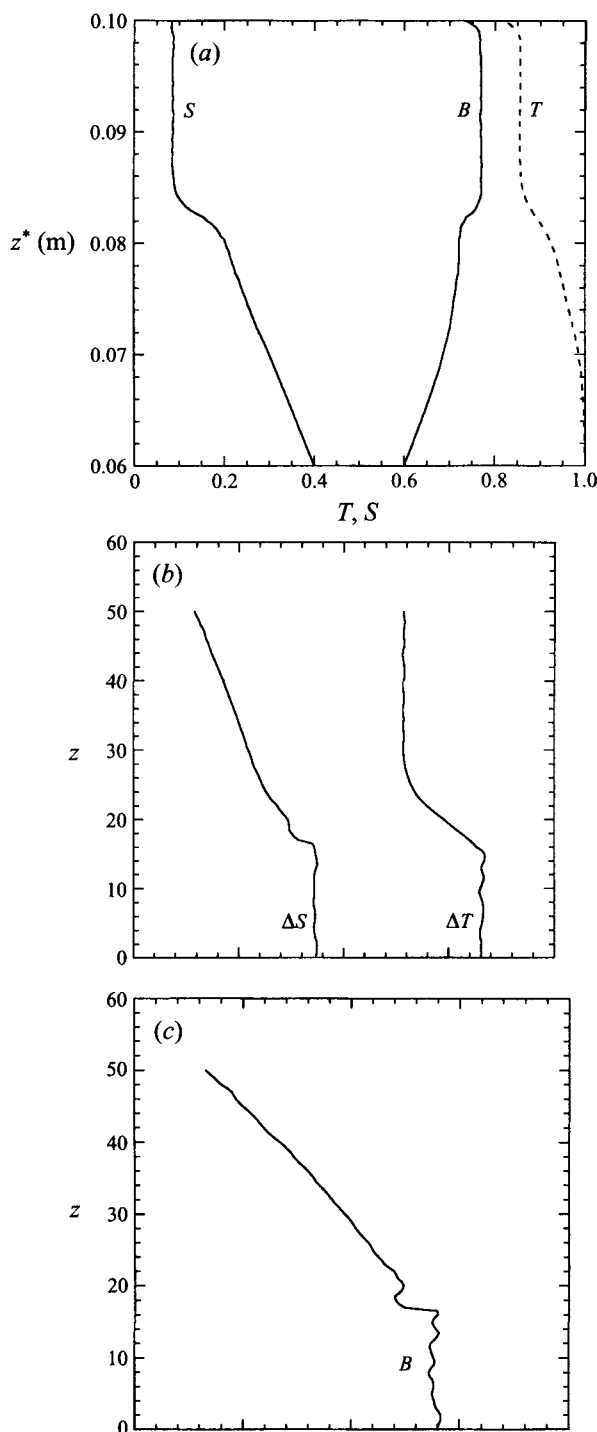


FIGURE 4. (a) Profiles of the horizontally averaged temperature, salinity and buoyancy at $t^* = 500$ s. (b) Reproduction of figure 9 from Huppert & Linden (1979) using a digital scan of the original paper. The scales $\Delta S, \Delta T$ indicate equal (but opposite) contributions to the buoyancy. The vertical coordinate z is non-dimensional (from Huppert & Linden 1979). (c) Vertical profile of the buoyancy, constructed by adding the temperature and salinity profiles of (b).

it does not rule out a non-zero buoyancy jump before the thermal boundary layer ahead of the interface becomes unstable.

3.1.3. Formation of the second layer

For $t^* > 500$ s there is some mixing underneath the first layer (figure 2), either caused by eddies which break through the interface or by eddies which are viscously driven by the deformation of the interface. Although the amount of 'pre-mixing' is small, it does have an effect on the development of the first layer. By transporting salt below the interface upward it enhances the buoyancy jump at the interface, slowing down the growth of the first layer. An additional effect of the 'pre-mixing' is an erosion of the salinity gradient underneath the first layer. Due to the much smaller diffusion coefficient the salt gradient recovers only very slowly back to its diffusion solution, whereas the (de-stabilizing) temperature gradient remains mostly intact. Due to this 'pre-mixing', convection may set in sooner, although it is not essential for the formation of the second layer. After sufficient time the destabilizing heat flux will always trigger an instability in the second layer and drive a convective flow.

When a second mixed layer is present, the convection in this layer will be able to work against the direction of migration of the interface and two evolution scenarios are possible. First, the second convecting layer is overtaken and entrained by the first through a break-up of the interface separating both layers (Fernando 1987). Although instabilities of the thermal boundary layer ahead of the interface occur throughout, they do not stop the first layer, because the mechanical mixing by the eddies prevents a stable interface forming between both layers. Only when the buoyancy jump is large enough, then the second layer remains separated from the first. Another possibility is that the second layer remains separated from the first but both layers migrate downward. The migration of the interface then stops at some later time. In an extreme case, the migration of the interface stops as soon as convection in the second layer is well developed. This has been observed by e.g. Turner (1968) and Huppert & Linden (1979). Both scenarios may occur in reality, and it requires additional analysis of the numerical results to understand these processes in more detail.

3.2. Relevant scales

In this section the growth rate of the first layer, the magnitude of the vertical velocities in this layer and the heat flux through the interface during the development of the first layer are analysed. Moreover, the energy budgets (both potential and kinetic) are monitored along the trajectory computed.

3.2.1. Growth rate of the first layer

To estimate the thickness of the mixed layer we have to choose a criterion to determine the location of the interface. In figure 5a the horizontally averaged squared vertical velocity $\overline{(w^*)^2}$ – which is a measure of the intensity of vertical mixing – is shown at $t^* = 2170$ s. From this figure, it is observed that $\overline{(w^*)^2}$ has a maximum in the first mixed layer and a smaller local maximum in the second layer. The layers are separated by a minimum of $\overline{(w^*)^2}$ (in figure 5(a) located at $z^* = 0.064$ m) coinciding with steep gradients in S and T . The location of this minimum is used as a measure of the thickness h^* of the first layer. Results for h^* versus time t^* are plotted in figure 5(b). Clearly oscillations can be seen during the evolution. Similar oscillations were found in the experiments of Turner (1968). The time scale of the oscillation in the computations is about 700 s, whereas in Turner (1968) it is about half this value.

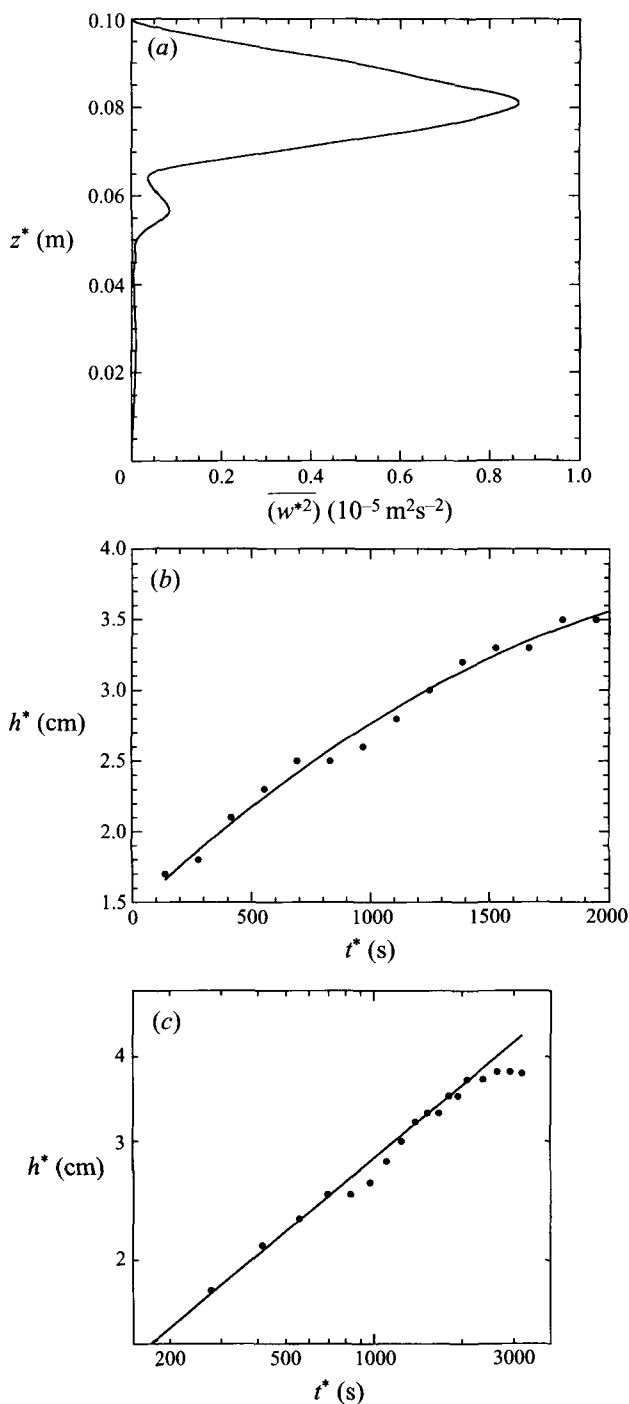


FIGURE 5. (a) A snapshot of the horizontally averaged intensity of vertical mixing $\overline{(w^*)^2}$ at $t^* = 2170$ s. The minimum located at $z^* = 0.064$ [m] coincides with the interface separating the first and the second layer. (b) The evolution of the thickness of the first layer h^* based on the minimum in $\overline{(w^*)^2}$ as shown in figure 5(a). (c) Same data as in (b) but plotted logarithmically and a power-law dependence is fitted.

This oscillation might be related to the original (oscillatory) diffusive instability which causes the initial convection. Also, it might be related to waves in the interface, which can be seen in an animation we made of the flow development. A third possibility is that the oscillation is caused due to the appearance of potential second mixed layers. These are entrained into the first layer, because the available energy for entrainment is still sufficiently large. However, due to advective salt transport below the interface, the activity in the second layer raises the buoyancy difference thereby giving a smaller growth rate. As the second layer is entrained into the first layer – thereby mixing the extra salt – the buoyancy difference becomes relatively smaller giving a faster growth. The period found in Turner (1968) is smaller probably because the experimental initial salinity gradient is larger.

In figure 5(c), the relation between h^* and t^* is replotted logarithmically. Both experiments and our numerical results show that the growth rate decreases with increasing time. It is clear that h^* increases with t^* at a smaller rate than $(t^*)^{1/2}$. Our best fit to the initial growth is a power-law dependence with exponent 0.36. The exponent proposed in Fernando (1987) to fit the experimental data is slightly larger. However, when the experimental results are considered in more detail, quite a range of power dependencies would fit the data of figure 4 in Fernando (1987). A power 0.5 as proposed in Fernando (1987) overestimates the overall growth rate for the range of q_0 and N shown.

3.2.2. Vertical velocity scaling

A scaling for the r.m.s. vertical velocity in terms of the imposed buoyancy flux q_0 at the boundary has been proposed by Hunt (1984):

$$(\overline{w^*})^2{}^{1/2} = c_0(q_0 h^*)^{1/3}, \quad (3.1)$$

where we interpret h^* as the thickness of the mixed layer and c_0 denotes an $O(1)$ constant. The maximum of $(\overline{w^*})^2{}^{1/2}$ is considered as a typical scale for this quantity and plotted as a function of time in figure 6. In the well-developed regime, a value of $(\overline{w^*})^2{}^{1/2} \approx 2.5 \times 10^{-3} \text{ m s}^{-1}$ is found. With $q_0 = 10^{-6} \text{ m}^2 \text{ s}^{-3}$ and $h^* \approx 3 \times 10^{-2} \text{ m}$ we find $(q_0 h^*)^{1/3} \approx 3 \times 10^{-3} \text{ m s}^{-1}$ implying that c_0 is indeed $O(1)$, giving support for the scaling (3.1). The fluctuations in the graph of $(\overline{w^*})^2{}^{1/2}$ increase during the development of the mixed layer. The convective eddies increase in size during the growth of the mixed layer and at later stages they have a size comparable to the width of the container. Therefore the fluctuations in these eddies are not averaged out over the width of the container as is the case in the beginning of the simulation.

3.2.3. Interfacial heat flux

In previously proposed simple models, often the diffusive heat flux through the interface was neglected during the growth of the mixed layer (Turner 1968; Huppert & Linden 1979; Fernando 1987). Our numerical results suggest that this might lead to significant errors in the prediction of the evolution of the first layer. In this section, the numerically calculated heat flux is compared with experimental results of heat fluxes through diffusive interfaces between convecting layers. Huppert (1971) proposed the following relation for the buoyancy (heat) flux $\overline{q_i}$ over a diffusive interface bounding two layers with a temperature and salinity difference. For the problem here (cooling from above), this expression becomes

$$\overline{q_i} = -c_1(\kappa/\nu)^{1/3}(-g\alpha\Delta\overline{T^*})^{4/3}(\alpha\Delta\overline{T^*}/\beta\Delta\overline{S^*})^2 \quad (3.2)$$

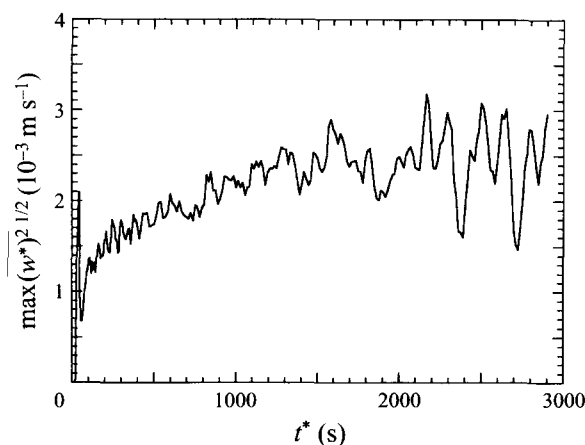


FIGURE 6. The evolution of the maximum of $(w^*)^2 / 2$ in time.

where $c_1 = 0.323$ and $\Delta \bar{T}^*$ and $\Delta \bar{S}^*$ are the horizontally averaged temperature and salinity differences over the interface. With the scaling as above, the non-dimensional heat flux becomes

$$\bar{F}_i = -c_1 Ra^{1/3} (-\Delta \bar{T})^{4/3} R_\rho^{-2} \quad (3.3a)$$

where $R_\rho = \alpha \Delta \bar{S} / (\beta \Delta \bar{T})$ is the buoyancy ratio over the interface. Similar relations for the diffusive heat flux have been proposed by Marmarino & Caldwell (1976) and Linden & Shirtcliffe (1978). Based on a different physical interpretation of the experimental results, Fernando (1989a) proposed another relation for the heat flux. For the problem here, the expression becomes

$$\bar{F}_i = -c_2 [Pr^{-1} Ra]^{1/5} (-\Delta \bar{T})^{6/5} \frac{(1 - \tau^{1/2} R_\rho)^{1/5}}{h_u^{2/5}} \quad (3.3b)$$

where $c_2 = 7 \times 10^{-2}$ and h_u is the thickness of the layer below the interface, i.e. the second layer. In figure 7, heat fluxes as calculated from the numerical results and as calculated from (3.3a) and (3.3b) are shown. The temperature and salinity differences were calculated from the jump over the interface in the horizontally averaged quantities. The error in the values as computed by both relations (3.3) can be quite large. A small error in $\Delta \bar{T}$ may easily lead to a large deviation in the calculated heat flux. Also, the value of h_u is not always well determined.

In particular at later times, when there is a convecting layer underneath the diffusive interface, there is a good correspondence between the numerical results and the heat fluxes obtained with either equation (3.3). Hence, when the growth of the first layer is small, the curves are close and the heat fluxes accurate up to 10%. This justifies the use of the heat flux formulations (3.3) in the one-dimensional model below. Either (3.3a) or (3.3b) could be used, but (3.3b) is not preferred because of the inaccuracy in h_u . In addition, figure 7 indicates that the heat flux through the interface cannot be neglected, having a value of about half the heat flux at the upper surface. Since the heat flux through the interface reduces the difference in temperature over the interface, the buoyancy jump increases. By ignoring the heat flux during the build-up of the layer, the buoyancy jump is underestimated which may lead to an overestimation of the growth rate of the first layer.

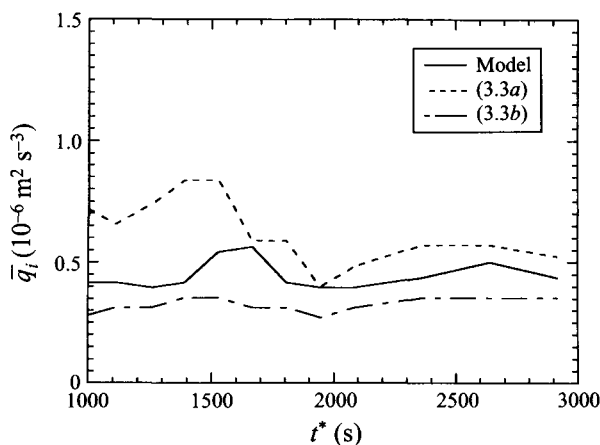


FIGURE 7. The buoyancy flux \bar{q}_i through the interface underneath the first mixed layer as a function of time. The flux is shown as calculated by the numerical model and as predicted by Huppert (1971) (3.3a) and Fernando (1989a) (3.3b).

3.2.4. Entrainment relation

In the simple model of Fernando (1987), an evolution equation for the layer thickness is used, which is obtained by considering a balance between the increase in potential energy due to mixing at the interface and the kinetic energy flux available at the interface. However, in this balance temperature differences were neglected. In the Appendix, an equation is derived for the rate of change of potential energy. Upon removing all the terms in this equation (A8) which are due to diffusion we find an expression for the rate of change in potential energy due to entrainment, i.e. in dimensionless form

$$\frac{d\langle E_p \rangle_e}{dt} = \frac{1}{2} \Delta \bar{B} h \frac{dh}{dt} \quad (3.4a)$$

where $\Delta \bar{B}$ is the horizontally averaged buoyancy jump across the interface, which incorporates temperature effects. An improved version of the entrainment relation used in Fernando (1987) therefore becomes

$$\frac{1}{2} \Delta \bar{B} h \frac{dh}{dt} = \tilde{\gamma} (\overline{w^2})^{3/2} \quad (3.4b)$$

where $(\overline{w^2})^{3/2}$ is the flux of kinetic energy at the interface and $\tilde{\gamma}$ is a mixing efficiency. Equation (3.4b) reduces to the entrainment relation suggested by Linden (1975) and used in Fernando (1987), when only contributions of salt to the buoyancy jump are considered. Relation (3.4b) can also be written as

$$\frac{u_e}{(\overline{w^2})^{1/2}} \sim Ri^{-1} \quad (3.4c)$$

where the Richardson number is defined as $Ri = \Delta B^* h^* / (\overline{w^2})^2$ and the entrainment velocity u_e has been defined as $u_e = dh/dt$. Relation (3.4c) has been frequently suggested in previous work (e.g. Linden 1975; Turner 1979; Hannoun, Fernando & List 1988).

We will return to this evolution equation later on, but only check in this section whether such a balance is found in the numerical results and, if yes, how large $\tilde{\gamma}$ must be chosen. For $\overline{w^2}$ we will use the parameterization for the convective velocity

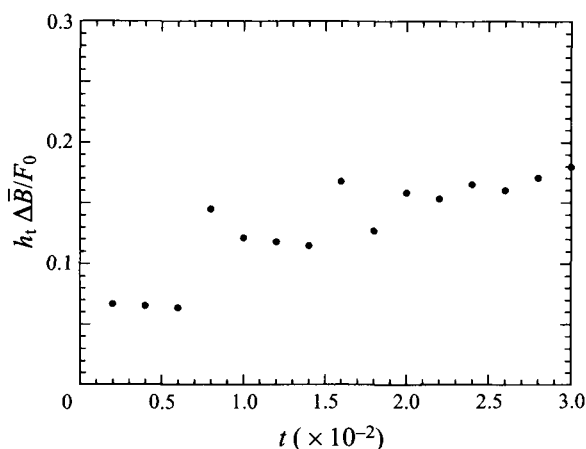


FIGURE 8. Check of the dimensionless entrainment relation (3.5) by plotting the expression for γ as a function of time t .

as discussed in §3.2.2. With (3.1), the balance (3.4c) becomes

$$\Delta \bar{B} \frac{dh}{dt} = \gamma F_0 \quad (3.5)$$

with $\gamma = 2\tilde{\gamma}$. Relation (3.5) is similar to the flux-ratio method which is used to predict the entrainment velocity of the free convecting atmospheric boundary layer (Stull 1976). In the atmospheric case, γ was found to have values between 0.1 and 0.3. The value for γ that is found from our numerical results is within this range. The ratio $\Delta \bar{B} (dh/dt)/F_0$ is plotted as a function of t in figure 8. Here dh/dt is computed from the fit of $h(t)$ plotted in figure 5(b) and $\Delta \bar{B}$ determined from the plots in figure 2. There is quite a spreading in the data in figure 8, but certainly at the later times the ratio is fairly constant with an average value of about 0.15. The slightly anomalous values for γ at small t are due to the fact that during the first stages of the evolution (small thickness of the mixed layer) the first layer is not yet fully turbulent.

3.2.5. Thickness of the interface

Many processes contribute to determine the evolution of the interface thickness h_i^* over which the stabilizing buoyant forces act, making it hard to find an exact relation. However, it is possible to obtain a lower bound for h_i^* , based on a straightforward consideration of the competition between diffusion and advection that determines h_i^* (Fernando 1989a). The length scale of the diffusive salinity boundary layer, i.e. the length scale of the stable buoyancy jump, is $(Dt^*)^{1/2}$ where t^* is a time scale over which the boundary can grow. For t^* , we use the turbulent time scale h^*/w^* , the mixed layer thickness and the convective velocity scale of the first layer and obtain

$$h_i^*/h^* = Pe^{-1/2}. \quad (3.6a)$$

The Péclet number Pe varies only slightly during the evolution of the mixed layer. Using values $D = 1.5 \times 10^{-9} \text{ m}^2 \text{ s}^{-1}$, $w^* = 2.5 \times 10^{-3} \text{ m}^2 \text{ s}^{-1}$ and $h^* = 3 \times 10^{-2} \text{ m}$ we obtain as a lower bound for the interface thickness

$$h_i^*/h^* \approx 0.4 \times 10^{-2}. \quad (3.6b)$$

The actual size of h_i^* will be larger for several reasons. The interface is not sandwiched between two convecting layers with comparable velocity and length scales, but

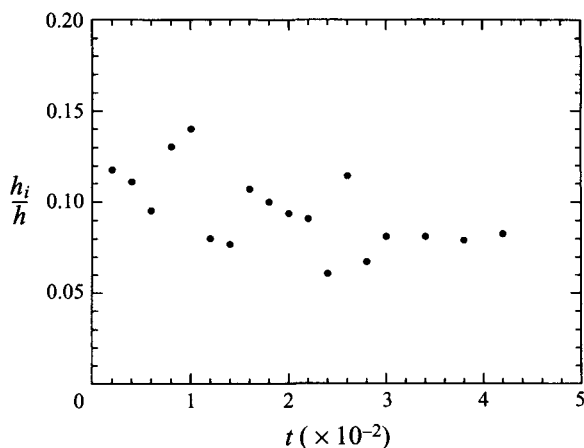


FIGURE 9. The ratio of interface thickness and layer thickness h_i/h against time t as obtained from horizontally averaged buoyancy profiles.

migrates into a region with almost quiescent fluid. Furthermore, the deformation of the interface, however minute, will also increase h_i^* . Available measurements suggest a constant fraction h_i^*/h^* (Fernando & Long 1985; Wolanski & Brush 1975) and a value $h_i^*/h^* = O(10^{-1})$. In figure 9, h_i^*/h^* is shown as obtained from the horizontally averaged buoyancy profiles in figure 2(d). The numerical predictions of the interface thickness are of the same order of magnitude as those reported from experiments and an estimate for the interface thickness is

$$h_i^* = 0.1 h^*. \quad (3.6c)$$

3.2.6. Energy budgets

In this section, we attempt to interpret the entrainment relation as well as the criterion for the final layer thickness directly from the calculation of the governing energy balances. Taking the inner product of \mathbf{u} with the momentum balance in primitive variables, an equation for the dimensionless kinetic energy E_k ($E_k \equiv \frac{1}{2}\mathbf{u}^2$) is obtained, i.e.

$$Pr^{-1} \frac{DE_k}{dt} = -\mathbf{u} \cdot \nabla p + \mathbf{u} \cdot \nabla^2 \mathbf{u} + wB \quad (3.7a)$$

where $B \equiv Ra(T - \lambda S)$ is the total buoyancy and D/dt the material derivative. The balance for the potential energy $E_p \equiv -zB$ is obtained by multiplying (2.1c) by $-zRa$, multiplying (2.1d) by $zRa\lambda$ and adding the result. This gives

$$\frac{DE_p}{dt} = -wB - Ra \left(\nabla^2(zT) - \tau\lambda \nabla^2(zS) - 2 \left(\frac{\partial T}{\partial z} - \tau\lambda \frac{\partial S}{\partial z} \right) \right) \quad (3.7b)$$

Both (3.7a) and (3.7b) can be integrated over the width of the domain ($x = 0$ to $x = A$) to get the horizontally averaged energy balances given by

$$Pr^{-1} \left[\frac{\partial \overline{E_k}}{\partial t} + \frac{\partial \overline{wE_k}}{\partial z} \right] = -\frac{\partial \overline{wp}}{\partial z} - \overline{\mathcal{D}} + \overline{wB} \quad (3.8a)$$

where $\mathcal{D} = \mathbf{u} \cdot \nabla^2 \mathbf{u}$ is the dissipation. For $\overline{E_p}$ (neglecting all terms proportional to τ) we obtain

$$\frac{\partial \overline{E_p}}{\partial t} + \frac{\partial \overline{wE_p}}{\partial z} = -\overline{wB} - Ra \frac{\partial}{\partial z} \left(z \frac{\partial \overline{T}}{\partial z} - \overline{T} \right). \quad (3.8b)$$

The globally averaged balances are obtained by integrating equations (3.8) vertically and applying the boundary conditions (2.3a–c), and we obtain

$$Pr^{-1} \frac{d\langle E_k \rangle}{dt} = -\langle \mathcal{D} \rangle + \langle wB \rangle, \quad (3.9a)$$

$$\frac{d\langle E_p \rangle}{dt} = -\langle wB \rangle - Ra(F_0 - T_{z=1} + T_{z=0}). \quad (3.9b)$$

All curves below were computed through time-averaging over a number of profiles near the times stated in the caption of each figure. As can be seen from (3.9a) there is a balance between the release of potential energy by the flow and viscous dissipation as long as the change in $\langle E_k \rangle$ is small. This is the case during the evolution of the diffusive interface (figure 10a). Both terms increase due to the constant input of heat at the top of the layer but keep the same order of magnitude. The increase of kinetic energy over the layer is an order of magnitude smaller.

In figure 10(b), the different contributions to the horizontally averaged kinetic energy balance (3.8a) are shown as a function of depth at $t^* = 500$ s. At this time, a second mixed layer has not yet developed. The buoyancy production in the mixed layer is approximately a linear function of depth and approaches the surface negative buoyancy flux at the surface ($F_0 = 10^6$ m² s⁻³). The dissipation is nearly constant over the mixed layer and nearly balances the buoyancy production at every level. The same terms are plotted in figure 10(c) at a later time $t^* = 2000$ s, when a second mixed layer is present. Within each layer, the same features are shown as presented above for only one mixed layer. Signatures of the interface, which is located near $z^* = 0.07$ m, are seen in figure 10(c) as a change in dissipation from one (near) constant value in the first layer to another (near) constant value in the second layer.

When (3.8a) is integrated from a level z to the surface, the energy surplus $\int_z^1 (wB - D) dz$ and the energy flux $(\overline{wE_k} + \overline{wp})$ at level z appear. These two terms are plotted in figure 10(d) at $t^* = 500$ s, corresponding to figure 10(b). The small imbalance between buoyancy production and dissipation, as seen in figure 10(b), is important. Integrated over the whole domain, it shows the trend of the volume averaged kinetic energy ($d\langle E_k \rangle/dt$), but at a particular depth this imbalance may be compensated by the energy flux $(\overline{wE_k} + \overline{wp})$. In figure 10(d), the energy flux is negative throughout the mixed layer (except at the surface). This indicates a downward flux of energy which at the bottom of the mixed layer is available for entrainment. The same quantities are shown at $t^* = 2000$ s in figure 10(e). The interface is located near the point where both energy surplus and energy flux change sign. In a small region below this interface the energy flux is positive (figure 10e) indicating a possible entrainment from the second layer upwards. The magnitude of this positive energy flux is much smaller than that in the first layer just above the interface.

Can the entrainment relation (3.5) be interpreted in terms of an energy balance? To investigate this, we consider the situation in figure 10(b), where the liquid below the interface is nearly motionless. Under the assumption that the first layer is well-mixed and the diffusive fluxes of salt can be neglected, it is shown in the Appendix that the

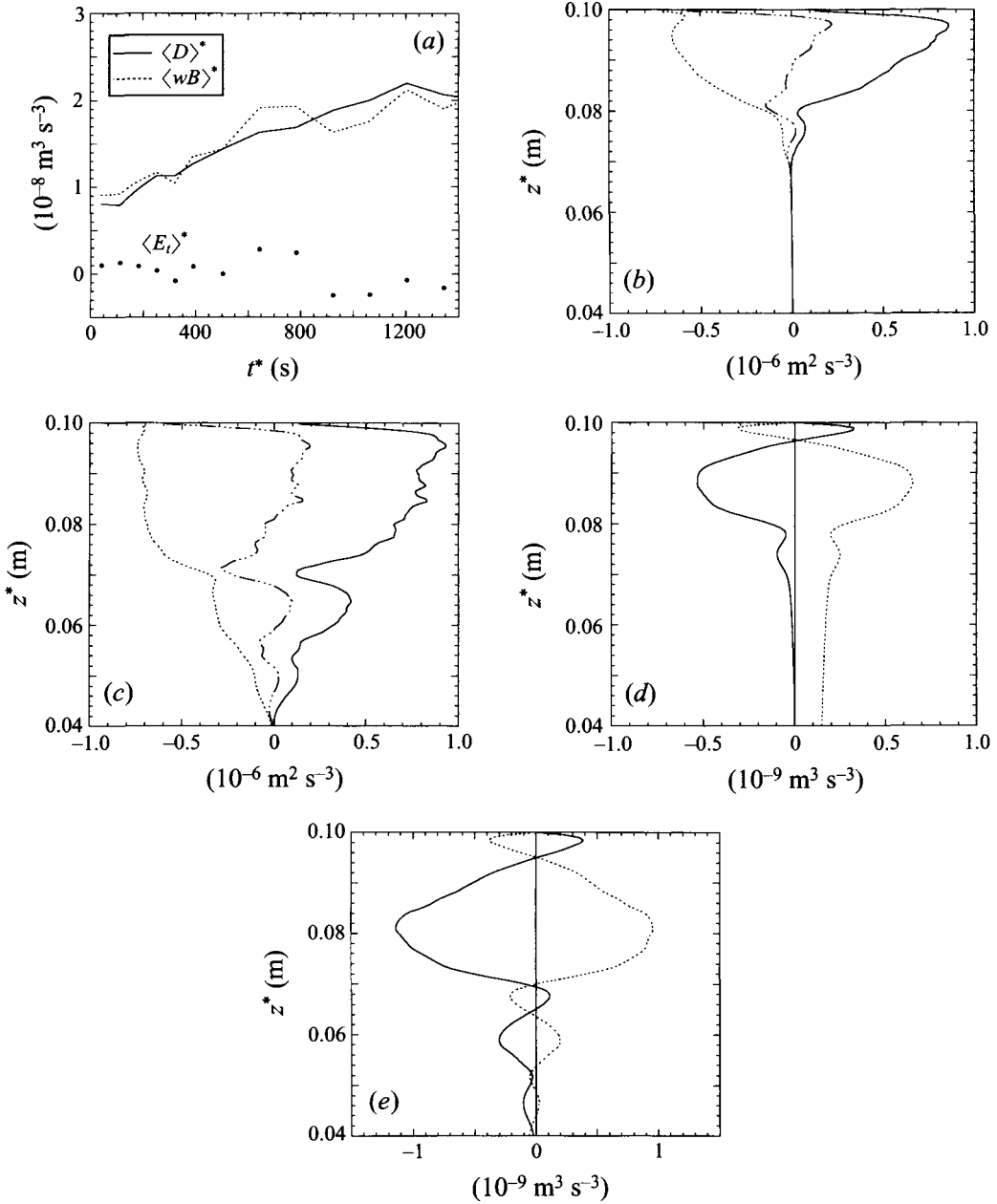


FIGURE 10. (a) Terms of the global kinetic energy balance as a function of time. Shown are the release of potential energy $\langle wB \rangle^*$, the dissipation $\langle \mathcal{D} \rangle^*$ and the time derivative of the total kinetic energy $\langle dE_k/dt \rangle^*$. (b) Horizontally averaged buoyancy production wB^* (solid), dissipation term \bar{D}^* (dashed) and divergence of vertical energy flux $\partial(wE_k^* + wp^*)/\partial z^*$ (dash-dotted) at $t^* = 500$ s. (c) Same as (b) but at $t^* = 2000$ s. (d) The energy surplus, $\int_{z^*}^H (wB^* - \bar{D}^*) dz^*$ (dotted) and the energy flux $wE_k^* + wp^*$ (solid) at level z at $t^* = 500$ s. (e) Same as (d) but at $t^* = 2000$ s.

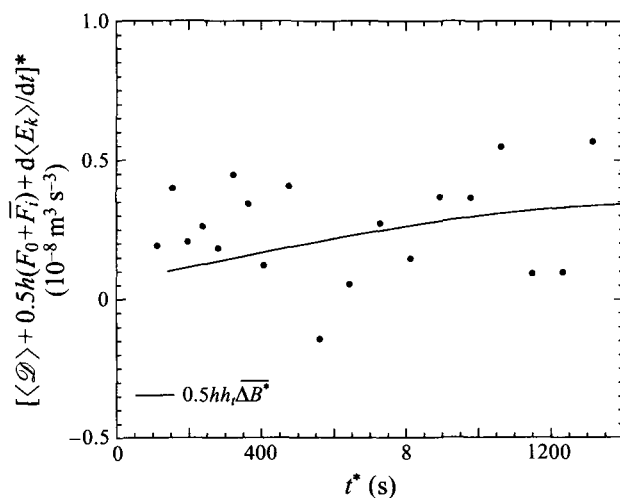


FIGURE 11. Check of the relation (3.10b) by plotting both sides of the equation (dimensional) as a function of time t^* (line is the left-hand side).

layer-integrated buoyancy production $\langle wB \rangle_m$ is given by

$$\langle wB \rangle_m = -\frac{1}{2}h \left(\Delta \bar{B} \frac{dh}{dt} + \bar{F}_i + F_0 \right) \quad (3.10a)$$

where \bar{F}_i is the heat flux through the interface. Substituting (3.10a) into the global kinetic energy balance (3.9a) and using the entrainment relation (3.5) (the layer below the mixed layer assumed motionless), we finally obtain an equation for the mixing efficiency γ ,

$$\frac{1}{2}\gamma F_0 = -\frac{\langle D \rangle}{h} - \frac{1}{2}(\bar{F}_i + F_0) - Pr^{-1} \frac{d\langle E_k \rangle / dt}{h}. \quad (3.10b)$$

In figure 11, the term $\frac{1}{2}\gamma F_0 h$ – computed from the buoyancy difference and interface movement according to (3.5) – is plotted as a function of time. The right-hand side of (3.10b) multiplied by h computed directly from the numerical results is also plotted in figure 11. There is significant spreading in the data in figure 11. Although both the dissipation and the heat flux are accurately enough, their difference (which is small) is not. However, the solid line in figure 11 showing the left-hand side of (3.10b) is not in contradiction with the data.

The relation (3.10b) gives an interpretation of the mixing efficiency in terms of an available energy. The average thermal energy entering the mixed layer is given by the second term in the right-hand side of (3.10b). Most of this energy is dissipated over the layer (the first term in the right-hand side) and a fraction is used to raise the average kinetic energy of the layer (the third term in the right-hand side). The remaining energy, scaled as a fraction of F_0 , is used to entrain liquid into the mixed layer and can indeed be considered as a mixing efficiency γ .

3.2.7. Final thickness of the first layer

As is clear from figures 2 and 5(c), the growth of the interface decreases significantly at a particular stage in the evolution. According to the evolution scenario as proposed in Turner (1968) and Huppert & Linden (1979) the growth rate decreases to zero due to the entrainment below the interface caused by convection in the second layer.

There are two arguments why we think this cannot be the only process responsible for a substantial decrease in growth rate. First, in figure 10(e) the magnitude of this entrainment is measured through the positive energy flux just below the interface, which is found to be much smaller than the negative energy flux just above the interface, even if the second layer is well-developed. Second, following Kelley (1987) the migration speed e of an interface separating two convecting layers, considering only turbulent entrainment, may be estimated as

$$e = C_1(1 - \eta) \frac{F_0}{\Delta B} \quad (3.11)$$

where $\eta = F_i/F_0$ is the ratio of the heat flux through the interface F_i and the surface heat flux F_0 . From (3.11) it follows directly that the migration speed of the interface can only become small when the heat flux through the interface nearly equals the surface heat flux. In the present case, the interfacial heat flux is always smaller than the surface heat flux and η is never more than approximately 0.5.

Therefore something else has to be considered to explain why the first layer stops growing. In the view presented by Fernando (1987), a transition in entrainment regime at the interface occurs. It is known that relations (3.4) and (3.5) are not valid over the whole range of Ri but that the straight conversion of kinetic energy into potential energy, which is the rationale behind these entrainment relations, cannot be applied at high Ri . This is, for example, discussed in the work of Linden (1973) and Dahm, Scheil & Tryggvason (1989) where mixing is studied by impinging vortex rings on a sharp density interface. At large Ri the 'eddies' tend to flatten at the interface, as if they were colliding on a rigid surface. In Turner (1979), it is suggested that for very high Ri all mixing curves flatten out and will become independent of Ri .

Subsequent growth of the mixed layer depends on the nature of the transport processes near the interface, but these are by no means clear. In figure 12, the horizontally averaged Nusselt and Sherwood numbers, defined by

$$Nu = \frac{\kappa \overline{T_z} - \overline{wT}}{\kappa \overline{T_z}}; \quad Sh = \frac{D \overline{S_z} - \overline{wS}}{D \overline{S_z}} \quad (3.12)$$

are plotted at $t^* = 500$ and 2000 s. These quantities measure the ratio of total vertical flux to the diffusive flux. A value near unity signifies purely diffusive transport whereas a large value indicates convectively dominated fluxes. From figure 12 it is clear that, as expected, Nu and Sh are very large in the mixed layer. From figure 12(a) it is seen that ahead of the first layer, Nu is $O(1)$ indicating a diffusive dominated heat transport whereas Sh is $O(10)$. During the growth of the first layer the transport of salt over the interface is therefore still convectively dominated. For $t^* = 2000$ s the value of Sh near the interface is significantly decreased ($Sh \approx 2$), indicating a transition in transport mechanism through the interface to a diffusively dominated regime.

In earlier studies (Fortescue & Pearson 1967; Turner 1979; Fernando & Long 1985; Crapper & Linden 1974) it has been suggested that the nature of the interfacial layer depends on the value of a local Péclet number. At large Pe , the interfacial layer consists of sporadically breaking waves which contribute to the interfacial mixing, whereas at small Pe , the interfacial layer is purely diffusive. The results in figure 12 suggest that the value of the appropriate local Péclet number is small, but it is not obvious how to define the actual scales since a thorough knowledge of the mixing processes is not available.

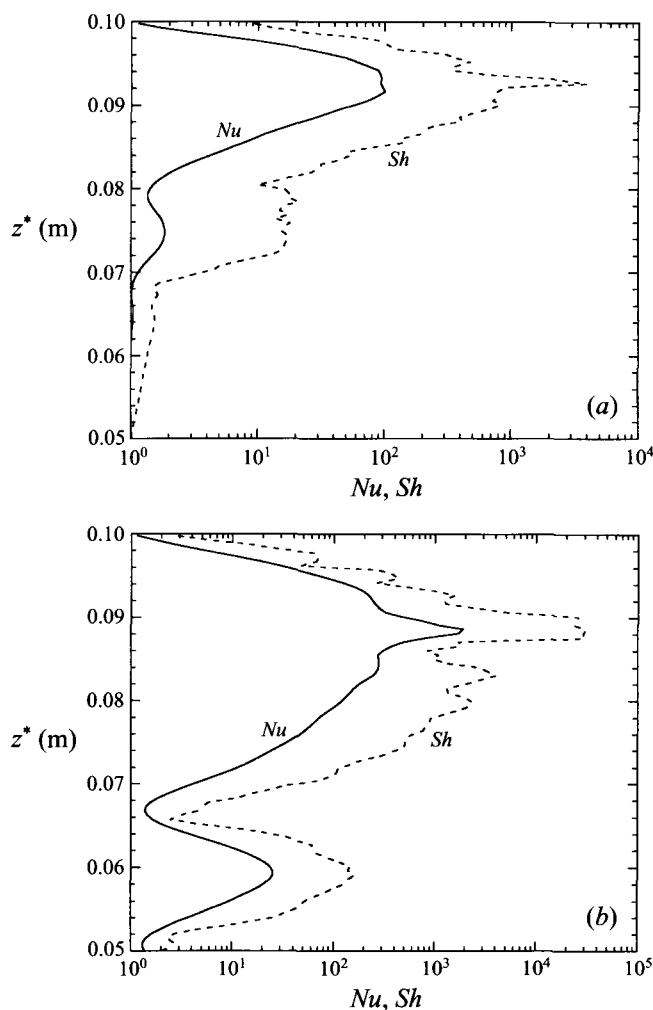


FIGURE 12. Horizontally averaged Nusselt (solid) and Sherwood (dashed) numbers, as defined in (3.12), as a function of height. (a) $t^* = 500$ s. (b) $t^* = 2000$ s.

An important question is what balance determines the transition between the turbulent entrainment regime and the diffusively controlled entrainment regime. Fernando (1987) suggests that this transition can be found from

$$\overline{(w^*)^2} = c_3 \overline{\Delta B^*} h^* \quad (3.13a)$$

which represents a balance between kinetic energy flux due to the eddies impinging on the interface and potential energy production associated with opposing buoyancy forces (Long 1978). In Fernando (1987), $\overline{\Delta B^*}$ is assumed to be the characteristic buoyancy variation of the eddies in the mixed layer. From figure 5(c) we find that the first layer reaches its final depth at $t^* \approx 2500$ s. It is at this moment that the balance (3.13a) should be valid. From figure 6 we find $\overline{(w^*)^2} \approx 10^{-5} \text{ m}^2 \text{ s}^{-2}$ and from figure 2(c) that $\overline{\Delta B^*} \approx 1.5 \times 10^{-2} \text{ m s}^{-2}$. With $h_f^* = 3.7 \times 10^{-2} \text{ m}$ we get a value $c_3 \approx 2 \times 10^{-2}$ giving no support for (3.13a) as a dominant balance. However, (3.13a) is best interpreted as a transition Richardson number between the two entrainment

regimes. Indeed, from the numerical results one finds that Ri increases during the growth of the first layer from $Ri \approx 40$ to a final value $Ri = c_3^{-1} \approx 10^2$ which is comparable to the value for Ri found in Hannoun & List (1988) for the transition to the regime that is controlled by diffusion.

One can try to modify (3.13a) to a relation which can be interpreted as a dominant energy balance. From the data in figure 2(d), we observe that buoyancy variations within the mixed layer are very small. The major part of the buoyancy variations occur over the interface separating the mixed layer from the underlying fluid. A different balance can therefore be proposed based on the interface thickness h_i^* as a characteristic value over which the buoyancy variations occur. This gives

$$\overline{(w^*)^2} = c_4 \overline{\Delta B^*} h_i^* \quad (3.13b)$$

where c_4 is a dimensionless constant which should be $O(1)$. Again from figure 2(c), we obtain $h_i^* \approx O(3 \times 10^{-3})$ m, and using the same values for $\overline{(w^*)^2}$ and $\overline{\Delta B^*}$, with (3.13b) it follows that $c_4 \approx 0.2$. This balance then expresses that there needs to be some minimum kinetic energy flux to deform an interface with thickness h_i^* and buoyancy jump ΔB^* .

4. A new one-dimensional model of layer formation

The numerical results give information on the dominant balances during the first stages of layer formation. Using this information, we try to improve on previously constructed one-dimensional models (Huppert & Linden 1979; Fernando 1987). In this section, a new model is proposed which is qualitatively in agreement with the dominant balances and can be quantitatively verified using the numerical results. The main idea behind the new model is a simple representation of the two entrainment regimes that are discussed in the previous section using a transition between the two regimes that is determined by (3.13a). The underlying assumptions of the model (of which most are verified in previous sections) are

- (1) all quantities are horizontally homogeneous;
- (2) temperature and salinity are constant over the first (mixed) layer and indicated below by T_m and S_m ;
- (3) all diffusive fluxes of salt can be neglected during the growth of the first layer;
- (4) the diffusive heat flux through the interface is given by (3.3a);
- (5) the liquid below the first mixed layer is motionless up to the point when the critical value of Ri is reached, given by (3.13b).

The starting point of the model is the evolution equation (3.5) for the mixed layer thickness, which describes the entrainment rate of the mixed layer from stably stratified surroundings. Integrating the equation for temperature (2.1c) (horizontally averaged) over the depth of the mixed layer leads to the following equation for the evolution of the mixed layer temperature T_m :

$$h \frac{dT_m}{dt} = -\Delta \overline{T} \frac{dh}{dt} + F_0 - \overline{F}_i \quad (4.1a)$$

where \overline{F}_i is the (horizontally averaged) diffusive heat flux through the interface, given by (3.3a). Because we neglect all diffusive fluxes of salt, the salinity of the mixed layer is given by

$$S_m = \frac{1}{2} h. \quad (4.1b)$$

Whereas the salinity profile underneath the mixed layer remains unchanged, the temperature in the quiescent layer underneath the interface is determined by

$$\frac{\partial T}{\partial t} = \frac{\partial^2 T}{\partial z^2} \quad (4.2a)$$

together with the boundary conditions

$$z = -h(t) : \quad \frac{\partial T}{\partial z} = \overline{F}_i, \quad (4.2b)$$

$$z \rightarrow -\infty : \quad \frac{\partial T}{\partial z} = 0. \quad (4.2c)$$

The set of equations (4.1)–(4.2) is solved numerically using an implicit time integration scheme (Crank–Nicolson) and central spatial differences. This method is second-order accurate in both time and space. To solve (4.2) numerically a coordinate transformation $z' = z + h(t)$ is used to handle the moving boundary at $z = -h(t)$. The magnitude of the time step and spatial grid size have been chosen to give sufficient accuracy. As initial conditions at $t = t_0$, a well-mixed layer with thickness $(\pi \kappa t_0^*)^{1/2}$ and a temperature T_m and salinity S_m which are found using the overall heat and salt balances are taken. The rationale behind these initial conditions is the instability of the thermal boundary layer with a thickness equal to the penetration depth $(\pi \kappa t_0^*)^{1/2}$. When the local effective Rayleigh number in this boundary layer (calculated using the temperature change over the boundary layer) is of the order 10^3 , this boundary layer will be unstable to (oscillatory) instabilities (Baines & Gill 1969). Several tests showed that the model is not sensitive to the thickness of this boundary layer as long as it is small. Equation (3.13b) is used to determine when the first mixed layer stops growing.

The one-dimensional model contains two coefficients. These are the mixing efficiency γ , and the coefficient c_4 in equation (3.13b). Numerical results have already provided estimates for these coefficients, with $\gamma \approx 0.1$ and $c_4 \approx 0.2$. For $\gamma = 0.11$ and $c_4 = 0.23$ the best agreement between the predictions of the one-dimensional model and the numerical results is obtained. The time evolution of the salinity S_m , the temperature T_m of the mixed layer and T_i , the temperature directly underneath the interface, are plotted in figure 13(a). The same quantities as calculated from the numerical simulation are shown as dots, showing a good agreement.

In figure 13(b) the layer thickness h^* versus time t^* is shown for two different values of q_0 . The solid line corresponds with the q_0 value of our numerical run and gives as best fit a power-law dependence with exponent 0.37. Also the point at which the relation (3.13b) is satisfied is indicated in the figure. In agreement with the results from the numerical simulation, the model predicts a layer growth at a smaller rate than a square-root dependence. The exponent increases with increasing q_0 to 0.42 at $q_0 = 0.04 \text{ cm}^2 \text{ s}^{-3}$. A larger cooling rate leads to a colder mixed layer and therefore a larger temperature difference. Although this both influences the interfacial heat flux and decreases the buoyancy jump, it apparently is the latter effect which dominates and leads to a larger growth rate.

Using the values for γ and c_4 as above, the parameter dependence of the final layer thickness h_f^* on q_0 and N is investigated and compared with experimental results in Fernando (1987) (his figures 5 and 6). The results of this comparison are shown in figure 14 where the points in the plot are from Fernando (1987) and the solid line is the prediction from the model. From figure 14(a) we conclude that the model results fit the experimental data quite well and a power-law dependence on N

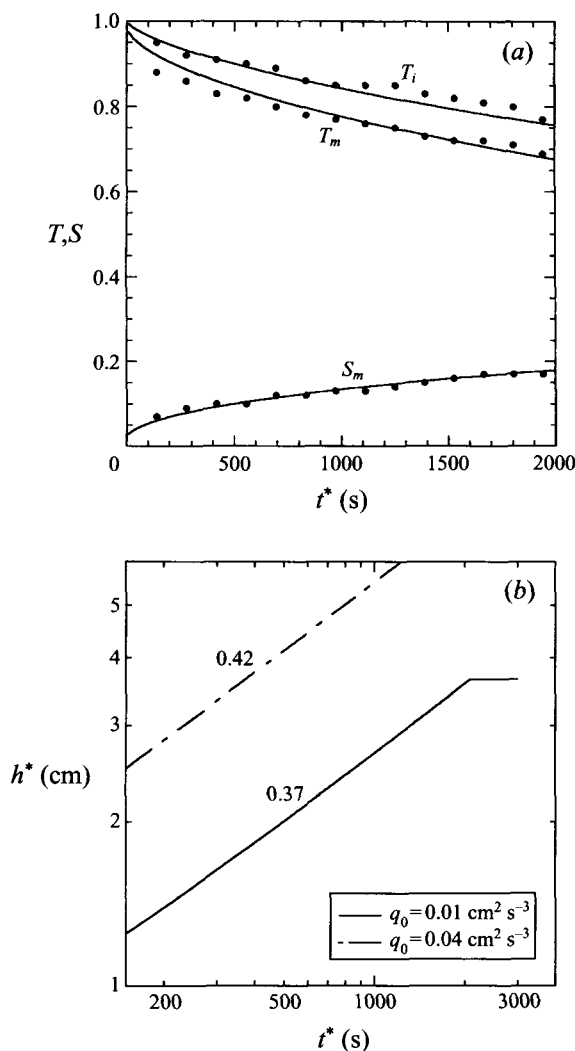


FIGURE 13. (a) T_m , S_m and the temperature directly underneath the interface T_i as calculated by the direct numerical simulation. Lines show the result of the one-dimensional model with $\gamma = 0.11$. (b) The growth rate of the first layer as calculated by the one-dimensional model for two values of q_0 . The thickness becomes constant (only shown for $q_0 = 0.01 \text{ cm}^2 \text{ s}^{-3}$) when the criterion (3.13b) is satisfied with $c_4 = 0.23$.

with $m = -1.56$ is found. This value is slightly more negative than that proposed in Fernando (1987). The exponent is not sensitive to the values of γ and c_4 as is demonstrated in figures 14(b) and 14(c). A similar comparison for the dependence on q_0 gives a good agreement with the experimental data. In fact, a slightly larger power $n = 0.53$ is found (figure 15a) than that proposed in Fernando (1987). The sensitivity to γ is again fairly weak (figure 15b), but slightly greater to c_4 (figure 15c). A smaller γ leads to a larger temperature difference, because there is less mixing. Hence the buoyancy jump is decreased and the final layer thickness becomes larger. A larger c_4 also leads to a larger layer thickness which can be seen directly from (3.13b), when the dependencies of the buoyancy jump (approximately linear with h^*) and r.m.s. vertical velocity (approximately as $h^{*1/3}$) are considered.

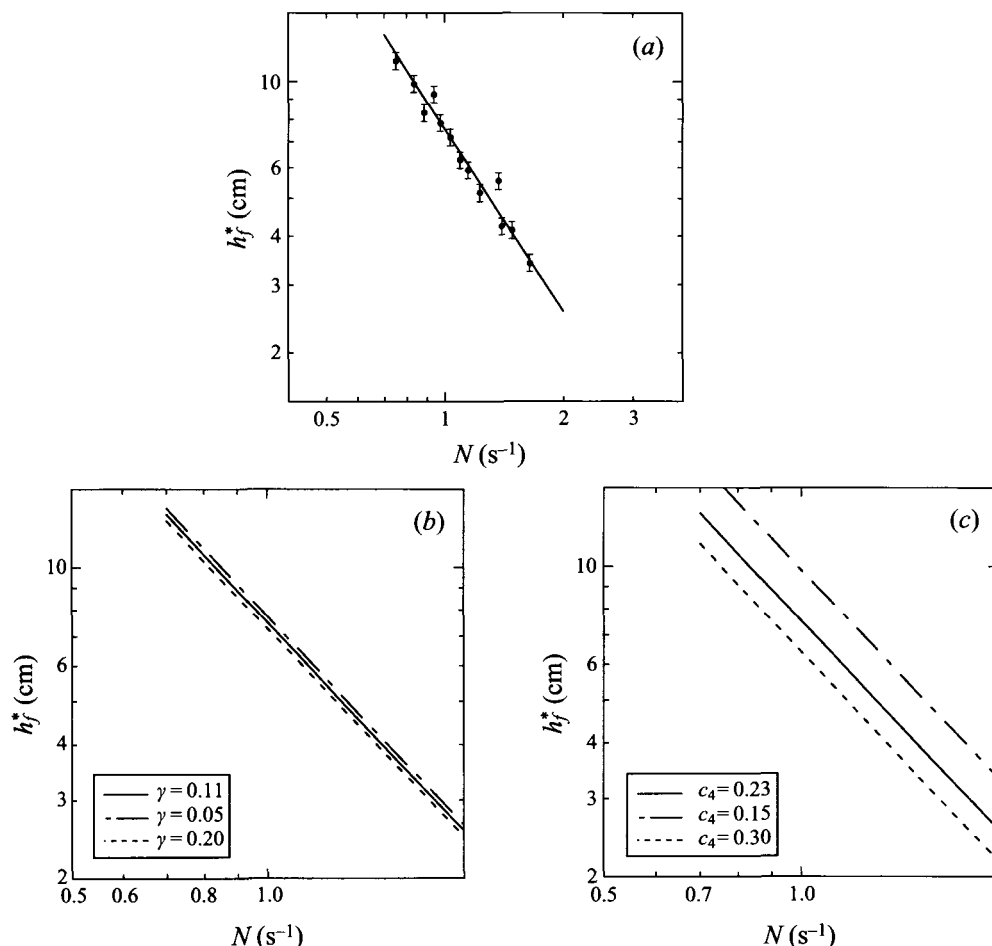


FIGURE 14. (a) Comparison of the calculations of the one-dimensional model for the dependence of h_f^* on N with the experiments in Fernando (1987). Dots are measurements taken from Fernando (1987), solid lines are the prediction of the model for $\gamma = 0.11$ and $c_4 = 0.23$. (b) Sensitivity of the relation in (a) to different values of γ . (c) Sensitivity of the relation in (a) to different values of c_4 .

5. Discussion

Based on the results above, the following physical description of the formation and evolution of a diffusive interface emerges. After cooling has started, the initial thermal boundary layer becomes unstable nearly instantaneously and vigorous convection develops. This leads to the formation of a well-mixed layer of thickness h which is initially small (of the order of the boundary layer thickness) but grows through turbulent entrainment.

The growth rate of the first layer is derived from the balance between the change in potential energy due to entrainment and the kinetic energy flux available at the interface, relation (3.4b). The latter was shown to be consistent with the numerical results and the constant γ can be interpreted in terms of a (residual) available energy. The heat flux over the interface was shown to agree well with proposed relations based on experiments. It is non-negligible and increases the buoyancy jump compared to the case where it is neglected. The temperature difference will be larger in the latter case and consequently, a slower growth rate of the interface is found.

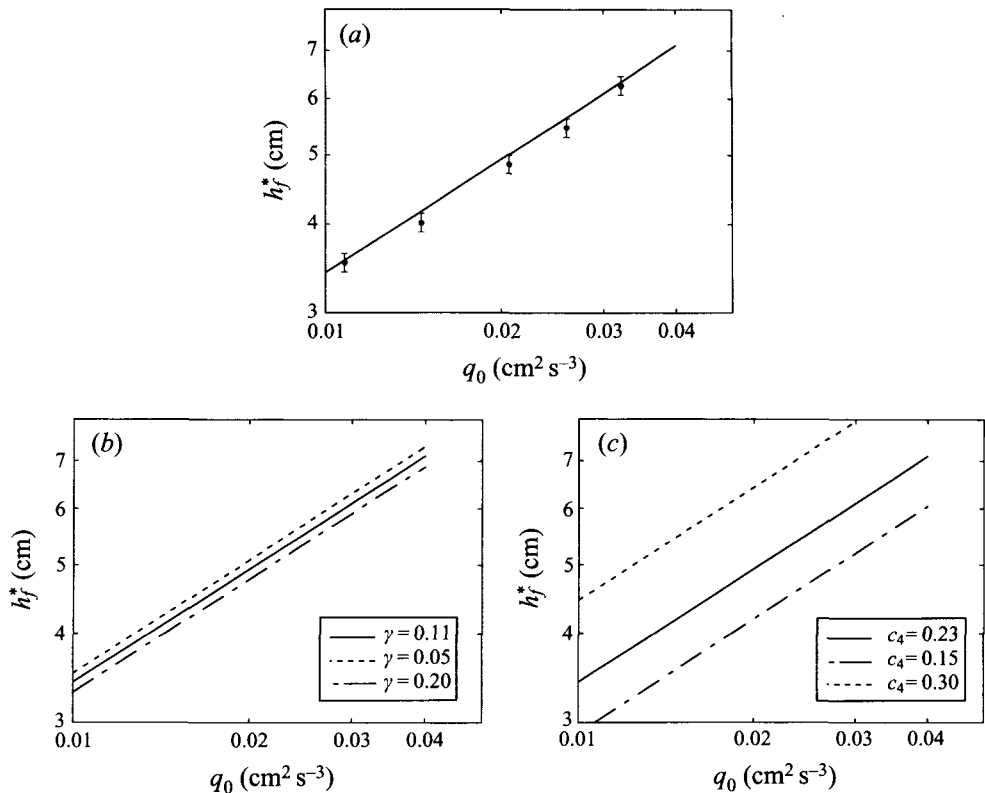


FIGURE 15. (a) Comparison of the one-dimensional model results with the experiments in Fernando (1987) for the dependence of h^* on q_0 . Dots are measurements taken from Fernando (1987), solid lines are the prediction of the model for $\gamma = 0.11$ and $c_4 = 0.23$. (b) Sensitivity of the relation in (a) to different values of γ . (c) Sensitivity of the relation in (a) to different values of c_4 .

Within the growth of this mixed layer downward, the r.m.s. vertical velocity scales as $h^{1/3}$ as proposed by Hunt (1984). There is a near balance between buoyancy production $\langle wB \rangle$ and dissipation $\langle \mathcal{D} \rangle$, and the mean kinetic energy of the layer does not change much (figure 10a). During the growth phase of the first layer, a downward energy flux just above the interface is available for entrainment (figure 10c).

In the simulation, we find clear evidence that there is a buoyancy jump $\overline{\Delta B}$ over the interface separating the mixed layer from the ambient liquid below, even if the thermal boundary layer ahead of this interface is still stable. When convection develops below the interface, the buoyancy jump increases simultaneously. The effect of salinity on this buoyancy difference is proportional to h . If ΔT becomes larger, the buoyancy difference is weakened. The intensity of the eddies increases with time as $h^{2/3}$, but the buoyancy jump $\overline{\Delta B}$ increases at a faster rate (approximately proportional to h). This causes the growth of the interface to decrease according to (3.4b), qualitatively in correspondence with experiments.

It was argued that the convective activity in the second layer cannot be solely responsible for stopping the growth of the first layer. Following Fernando (1987), a transition in entrainment regime is proposed as a mechanism to accomplish this. Eventually, the buoyancy jump will become large enough, such that the most energetic eddies will not be able to deform the interface. The growth of the mixed layer will

then become negligibly small. The final thickness of the first layer is then determined by the value of a critical Richardson number (3.13a). This can also be interpreted as an energy balance (3.13b), which shows that there needs to be some minimum kinetic energy flux to deform an interface with thickness h_i and buoyancy jump ΔB . As soon as the growth of the first layer has decreased significantly, a well-mixed second mixed layer appears. The interfacial transport of heat and salt was shown to be predominantly diffusive at that stage.

It is important to identify the essential double-diffusive features that are responsible for the multiple-layered structure. Or, in other words, why cooling a stable temperature gradient from above does not lead to the same multiple convecting layers that are separated by diffusive interfaces. For a second layer to be established separately from the first it is necessary to have a destabilizing gradient, due to the heat flux through the interface, to drive convection underneath the interface. However, it is of equal importance to have a very stable interface that separates the two layers, otherwise the second layer will just be entrained into the first mixed layer. It is here that the double-diffusive nature of the problem is crucial. It has been shown that both heat and salt fluxes over the interface are diffusively dominated. The flux of salt through the interface is small and the salinity jump over the interface remains intact. The heat flux through the interface, however, is much larger and is able to drive the flow in the second layer. It is the fact that simultaneously a destabilizing (heat) flux is coexisting with a sustained very stable interface that is responsible for the multiple-layered structure. Although in single-component experiments it is possible to show a diffusive controlled entrainment regime (Linden 1973; Hannoun & List 1988), one needs (at least) two components with different diffusion coefficients to obtain multiple convecting layers.

The improved knowledge of the evolution of a diffusive interface leads to a new one-dimensional model. This model improves on that in Fernando (1987) in that it takes into account the effect of the temperature jump across the interface on the entrainment rate. It uses the diffusive heat flux over the interface and the change in temperature in the ambient liquid to compute the temperature difference. Both effects are shown to be important for the evolution of the mixed layer thickness. The model predicts a power-law dependence m and n on N and q_0 , respectively with $m = -1.56$ and $n = 0.53$, which fit the experiments very good. This result is not sensitive to the choice of the two coefficients appearing in the model. The results for ocean mixing parameterizations as in Fernando (1989b) depend heavily on these exponents. Although these exponents are not very different than those proposed by Fernando, our one-dimensional model gives a more theoretical justification for their use.

The model can be easily extended to total staircase growth. When the first layer stops, the second layer starts, forced by a heat flux equal to the diffusive heat flux through the first interface. The evolution of the second layer follows mainly the same lines as that of the first layer. One should, however, monitor the ratio of the destabilizing heat flux over subsequent interfaces. If these are nearly equal the effect of convection in the subsequent layer may be much more pronounced and the first layer may stop growing, even if the transition Richardson number has not been reached.

We thank one of the (anonymous) referees for persistent comments on the interpretation of the results presented, which lead to significant improvements of the paper. All computations were performed on the CRAY C98 at the Academic Computing Centre (SARA), Amsterdam, the Netherlands within the project SC212. Use of

these computing facilities was sponsored by the Stichting Nationale Supercomputer faciliteiten (National Computing Facilities Foundation, NCF) with financial support from the Nederlandse Organisatie voor Wetenschappelijk Onderzoek (Netherlands Organization for Scientific Research, NWO).

Appendix. Change in potential energy due to entrainment.

The starting point is the global potential energy balance (3.9b). We will assume that there is only release of potential energy in the mixed layer and the liquid underneath the layer is motionless, i.e.

$$\langle wB \rangle_m = Ra \int_{1-h}^1 (\overline{wT} - \lambda \overline{wS}) dz. \quad (\text{A } 1)$$

An explicit expression for $\langle wB \rangle_m$ is found as follows. The heat and salt equations (2.1c, d) averaged over the horizontal are

$$\frac{\partial \overline{T}}{\partial t} = \overline{T}_{zz} - (\overline{wT})_z \quad \frac{\partial \overline{S}}{\partial t} = \tau \overline{S}_{zz} - (\overline{wS})_z. \quad (\text{A } 2a, b)$$

In the (well-mixed) first layer, $\partial \overline{T} / \partial t = dT_m / dt$ is constant with depth

$$z \in [1-h, 1] : \quad \partial(\overline{T}_z - \overline{wT}) / \partial z = dT_m / dt \quad (\text{A } 3a)$$

or (integrating (A 3a)):

$$z \in [1-h, 1] : \quad \partial \overline{T} / \partial z - \overline{wT} = z(dT_m / dt) + C. \quad (\text{A } 3b)$$

Now the first term in the left-hand side is zero and the constant C is determined by the boundary conditions at the upper surface. This leads to an explicit expression for \overline{wT}

$$z \in [1-h, 1] : \quad \overline{wT} = -(dT_m / dt)(z-1) - F_0. \quad (\text{A } 3c)$$

Integrating (A 3c) from $z = 1-h$ to $z = 1$ gives an expression for $\langle wT \rangle_m$:

$$\langle wT \rangle_m = h \left[\frac{1}{2} h \frac{dT_m}{dt} - F_0 \right]. \quad (\text{A } 3d)$$

We are left with dT_m / dt as an unknown. Integrating (A 2a) in parts from $z = 0$ to $z = 1$:

$$\frac{\partial}{\partial t} \int_{1-h}^1 \overline{T} dz + \frac{\partial}{\partial t} \int_0^{1-h} \overline{T} dz = F_0. \quad (\text{A } 4)$$

Integrating (A 2a) from $z = 0$ to $z = 1-h$:

$$\frac{\partial}{\partial t} \int_0^{1-h} \overline{T} dz = -\overline{T}_i \frac{dh}{dt} + \overline{F}_i. \quad (\text{A } 5)$$

In (A 5), \overline{F}_i is the diffusive heat flux through the interface and \overline{T}_i the temperature directly underneath the interface. Using $\overline{T} = T_m$ in the mixed layer and (A 5), we can now write (A 4) as

$$h \frac{dT_m}{dt} = -\Delta \overline{T} \frac{dh}{dt} + F_0 - \overline{F}_i \quad (\text{A } 6)$$

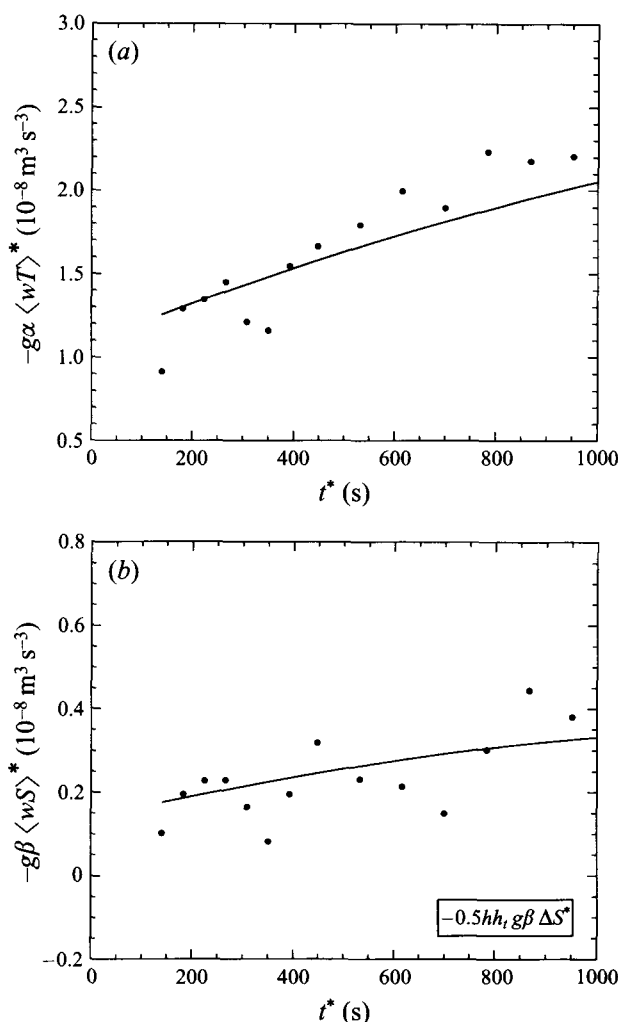


FIGURE 16. (a) Check of the dimensionless relation (A 7a) by plotting both sides of the equation (line is the right-hand side) as a function of time t . (b) Same as (a) but now for relation (A 7b).

where $\Delta \bar{T} = T_m - \bar{T}_i$. Substituting (A 6) into (A 3d) eventually gives

$$\langle wT \rangle_m = -\frac{1}{2}h \left[\Delta \bar{T} \frac{dh}{dt} + \bar{F}_i + F_0 \right]. \quad (\text{A } 7a)$$

In a similar way an expression for $\langle wS \rangle_m$ is derived:

$$\langle wS \rangle_m = -\frac{1}{2}h \Delta \bar{S} \frac{dh}{dt} \quad (\text{A } 7b)$$

where $\Delta \bar{S}$ is the salinity difference between both layers. Confirmation of the relations (A 7) was obtained from the numerical simulation. In figure 16, both $\langle wT \rangle$ and $\langle wS \rangle$ calculated directly from the numerical values are plotted together with the right-hand side of (A 7). Although there is significant spreading, both the order of magnitude

and the trends correspond. The expression for $d\langle E_p \rangle / dt$ from (3.9b) finally becomes

$$\frac{d\langle E_p \rangle}{dt} = \frac{1}{2} \Delta \bar{B} h \frac{dh}{dt} + Ra \left[\frac{1}{2} h (\bar{F}_i + F_0) - F_0 - \bar{T}_{z=1} + \bar{T}_{z=0} \right] \quad (\text{A } 8)$$

Only the first term on the right-hand side is related to entrainment and for later reference, we denote this term by $d\langle E_p \rangle_e / dt$. If only the effect of salt is considered, equation (A 8) reduces directly to the expression of Linden (1975), which is

$$\frac{d\langle E_p \rangle_e}{dt} = -\lambda Ra \frac{1}{2} h \Delta \bar{S} \frac{dh}{dt} = \lambda Ra \frac{1}{4} h^2 \frac{dh}{dt} \quad (\text{A } 9)$$

where $\Delta \bar{S} = -\frac{1}{2} h$ is used, as is the case when the initial salt gradient is linear.

REFERENCES

- BAINES, P. G. & GILL, A. E. 1969 On thermohaline convection with linear gradients. *J. Fluid Mech.* **37**, 289–306.
- CRAPPER, P. F. & LINDEN, P. F. 1974 The structure of the turbulent density interfaces. *J. Fluid Mech.* **65**, 45–63.
- DAHM, W. J., SCHEIL, C. M. & TRYGGVASON, G. 1989 Dynamics of vortex interaction with a density interface. *J. Fluid Mech.* **205**, 1–43.
- DIJKSTRA, H. A. 1988 Transient Marangoni convection in a square container. *PhysicoChem. Hydrodyn.* **10**, 493–515.
- FERNANDO, H. J. S. 1987 The formation of a layered structure when a stable salinity gradient is heated from below. *J. Fluid Mech.* **182**, 525–541.
- FERNANDO, H. J. S. 1989a Buoyancy transfer across a diffusive interface. *J. Fluid Mech.* **209**, 1–34.
- FERNANDO, H. J. S. 1989b Oceanographic implication of laboratory experiments on diffusive interfaces. *J. Phys. Oceanogr.* **19**, 1707–1715.
- FERNANDO, H. J. S. 1991 Turbulent mixing in stratified fluids. *Ann. Rev. Fluid Mech.* **23**, 455–493.
- FERNANDO, H. J. S. & LONG, R. R. 1985 On the nature of the entrainment interface of a two-layer fluid subjected to zero-mean-shear turbulence. *J. Fluid Mech.* **151**, 21–53.
- FORTESCUE, G. E. & PEARSON, J. R. A. 1967 On gas absorption into a turbulent fluid. *Chem Engng Sci.* **22**, 1163.
- GARGETT, A. E. & HOLLOWAY, G. 1992 Sensitivity of the GFDL ocean model to different diffusivities of heat and salt. *J. Phys. Oceanogr.* **22**, 1158–1177.
- HANNOUN, I. A., FERNANDO, H. J. S. & LIST, E. J. 1988 Turbulence structure near a sharp density interface. *J. Fluid Mech.* **189**, 189–209.
- HANNOUN, I. A. & LIST, E. J. 1988 Turbulence mixing at a shear-free density interface. *J. Fluid Mech.* **189**, 211–234.
- HUNT, J. C. R. 1984 Turbulence structure in thermal convection and shear-free boundary layers. *J. Fluid Mech.* **138**, 161–184.
- HUPPERT, H. E. 1971 On the stability of double-diffusive layers. *Deep-Sea Res.* **18**, 1006–1021.
- HUPPERT, H. E. & LINDEN, P. F. 1979 On heating a stable salinity gradient from below. *J. Fluid Mech.* **95**, 431–464.
- HUPPERT, H. E. & TURNER, J. S. 1981 Double-diffusive convection. *J. Fluid Mech.* **106**, 299–329.
- KAZMIERCZAK, M. & POULIKAKOS, D. 1990 Transient double diffusion in a stable stratified fluid layer heated from below. *Intl J. Heat Fluid Flow* **11**, 30–39.
- KELLEY, D. E. 1984 Effective diffusivities within ocean thermohaline staircases. *J. Geophys. Res.* **89**, 10484–10488.
- KELLEY, D. E. 1987 Interface migration in thermohaline staircases. *J. Phys. Oceanogr.* **17**, 1633–1639.
- LINDEN, P. F. 1973 The interaction of a vortex ring with a sharp density interface: a model for turbulent entrainment. *J. Fluid Mech.* **60**, 467–480.
- LINDEN, P. F. 1975 The deepening of a mixed layer in stratified fluid. *J. Fluid Mech.* **71**, 385–405.
- LINDEN, P. F. & SHIRTCLIFFE, T. G. L. 1978 The diffusive interface in double diffusive convection. *J. Fluid Mech.* **84**, 113–124.
- LONG, R. R. 1978 A theory of mixing in a linearly stratified fluid. *J. Fluid Mech.* **84**, 113–124.

- MARMORINO, G. O. & CALDWELL, D. R. 1976 Heat and salt transport through a diffusive thermohaline interface. *Deep-Sea Res.* **23**, 59–67.
- MOLEMAKER, M. J. & DIJKSTRA, H. A. 1995 Layer formation in a stably stratified liquid cooled from above. In *Double Diffusive Convection* (ed. A. Brandt & H. J. S. Fernando). Geophysical Monograph, vol. **94**, pp. 97–104.
- SCHMITT, R. W. 1994 Double diffusion in oceanography. *Ann. Rev. Fluid Mech.* **26**, 255–285.
- STULL, R. B. 1976 The energetics of entrainment across a density interface. *J. Atmos. Sci.* **33**, 1260–1267.
- TURNER, J. S. 1968 The behaviour of a stable salinity gradient heated from below. *J. Fluid Mech.* **33**, 183–200.
- TURNER, J. S. 1979 *Buoyancy Effect in Fluids*, 2nd Edn. Cambridge University Press.
- TURNER, J. S. & STOMMEL, H. 1964 A new case of convection in the presence of vertical salinity and temperature gradients. *Proc. Natl Acad. Sci.* **52**, 49–53.
- WOLANSKI, E. J. & BRUSH, L. M. 1975 Turbulent entrainment across stable density step structures. *Tellus* **27**, 259–268.